Multiple ultra-wideband signal sources exploiting XPM in SFRL*

ZHAO Zanshan**, **XING Weiguang, and GAN Weiming**
Haikou Lab, Institute of Acoustics, Chinese Academy of Sciences, Haikou 570100, China

(Received 21 June 2021; Revised 17 August 2021)

A novel scheme for all-optical broadcast ultra-wideband (UWB) monocycle pulses generation based on cross-phase modulation (XPM) in semiconductor fiber ring laser (SFRL) is proposed, in which three UWB positive or negative monocycle pulses can be generated simultaneously. A comprehensive broad-band dynamic model for this kind of all-optical broadcast UWB monocycle sources is established, which is further applied to numerically analyze the impacts of injection current of semiconductor optical amplifier (SOA), the power and wavelength of the signal light on the performance of the UWB positive monocycle pulses with higher power spectral density. The results show that the spectra of the UWB positive and negative monocycle pulses generated by this scheme match the Federal Communications Commission (FCC) definition quite well. Three UWB positive monocycle pulses with better performance can be obtained when the power of signal light is at a high level, and three other UWB positive monocycle pulses with good tolerance to both the injection current of the SOA and the wavelength of the signal light can be obtained. In addition, the powers of the lasing light coupled into the SFRL should not be strong to obtain three UWB positive monocycle pulses with better performance.

Document code: A **Article ID:** 1673-1905(2022)02-0077-8
DOI https://doi.org/10.1007/s11801-022-1098-6

Ultra-wideband (UWB) technology is considered as a promising solution of short-range broadband wireless communication and sensor network because of its superior advantages, such as lower power consumption, higher bit rate, immunity to multipath fading, shorter time duration, and lower duty cycle[1,2]. According to the Federal Communications Commission (FCC), UWB signal should have a 10 dB bandwidth larger than 500 MHz or a fractional bandwidth greater than 20%, and the power spectral density (*PSD*) of the frequency range from 3.1 GHz to 10.6 GHz is restricted below −41.3 dBm/MHz[3]. The UWB signal is limited to short distances due to its low power density. In order to extend the transmission distance of the UWB signal, UWB over fiber has been proposed, and the methods of generating UWB signal in optical domain have been investigated.

Various approaches for generating the UWB signals in optical domain have been proposed, such as using the radio frequency signal to modulate the laser directly to obtain the UWB signals[4], using the frequency-to-time mapping principle to generate the UWB monocycle and doublet pulses[5], based on phase modulation to intensity modulation (PM-IM) conversion to produce the UWB pulses[6-8], and generating the UWB monocycle and doublet pulses by combining a pair of polarity-reversed Gaussian pulses with appropriate time delay[9-13]. In addition, there are also some other methods for generating UWB signals, such as the UWB monocycle and doublet pulses can be obtained through photon echo in rare earth-doped optical crystal[14], and using up-conversion based on stimulated Brillouin scattering effect[15].

The schemes of generating UWB signals in optical domain are mainly for producing single signal. To the best of our knowledge, there are three papers reported to generate multiple UWB signals simultaneously[16-18]. In this paper, we propose a novel scheme for all-optical broadcast UWB monocycle pulses generation based on cross-phase modulation (XPM) in semiconductor fiber ring laser (SFRL), in which three UWB positive or negative monocycle pulses can be generated at the same time. Since our scheme use semiconductor optical amplifier (SOA) as non-linear medium, the structure is simpler than the one proposed in Ref.[16]. Compared with Refs.[17,18], our solution can generate two kinds of UWB monocycle pulses just by adjusting the frequency offset of the filters. We establish the comprehensive broad-band dynamic model of this kind of all-optical broadcast UWB signal sources. Using the comprehensive broad-band dynamic model, we generate three UWB positive and negative monocycle pulses and analyze the impacts of the current of the SOA in the SFRL, the power and wavelength of the signal light on the three

* This work has been supported by the Hainan Provincial Natural Science Foundation of China (No.620MS078).
** E-mail: zhaozanshan@163.com

UWB positive monocycle pulses.

The scheme of all-optical broadcast UWB monocycle pulses based on XPM in the SFRL is shown in Fig.1. The SFRL is consisted of an SOA, two optical couplers (OCs), two optical polarization controllers (PCs), an optical isolator, and an optical comb filter. The SOA is the gain medium of SFRL. The optical isolator is used to prevent the reflection. Two PCs whose polarization directions are perpendicular to each other were used to set the polarization direction of lasing light and signal light, avoiding the four-wave mixing (FWM) effect between signal light and laser light in SOA. The optical comb filter is used to select the wavelengths of lasing light. The signal light and lasing light are input to the SOA through the OC1. The phase of a lasing light is modulated by the signal light through the XPM in the SOA. The chirp of a lasing light is the first order derivative of the phase, which has a monocycle shape. The monocycle pulse can be obtained by using a Gaussian optical bandpass filter (OBF) to convert the chirp into amplitude. Two polarity-reversed UWB monocycle pulses can be obtained by setting the central wavelength of the OBF to be red shifted or blue shifted. By setting the number of the comb filter channels, multi-channels of the UWB monocycle pulses can be generated.

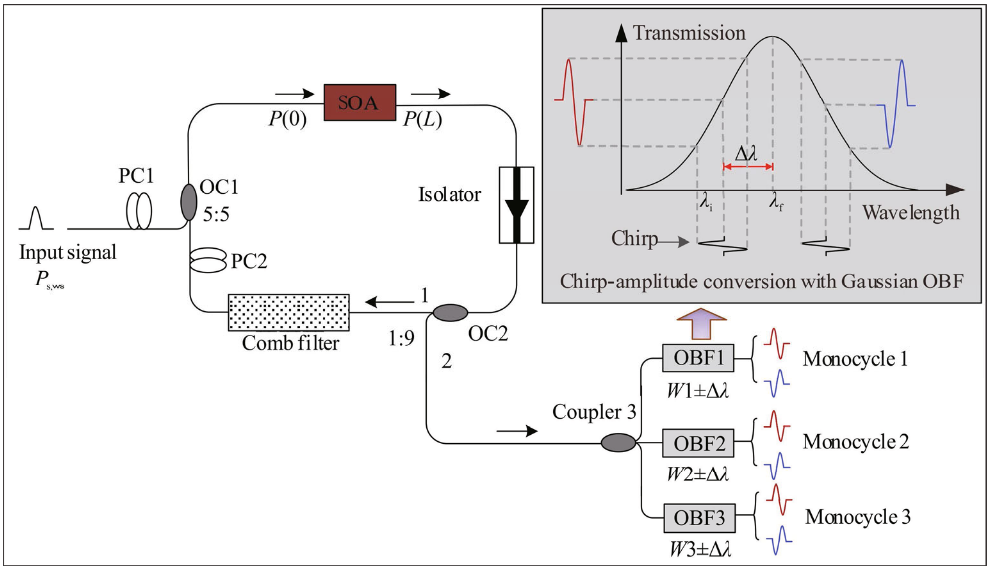

Fig.1 Scheme of all-optical broadcast monocycle signal sources based on XPM in SFRL

The SOA in the SFRL is not only the gain medium, but also the nonlinear medium. In the simulation, the SOA is divided into many small sections. The evolution of the slowly varying amplitude A inside SOA obeys the traveling-wave equation[19]

$$\frac{\mathrm{d}A_{k,\mathrm{i}}}{\mathrm{d}z}=\frac{1}{2}\left[\frac{\Gamma g_{k,\mathrm{i}}}{1+P_{\mathrm{i}}/P_{\mathrm{sat}}}(1-\mathrm{i}\alpha_{k,\mathrm{i}})-\alpha_{\mathrm{int}}\right]A_{k,\mathrm{i}}+\mu_{k,\mathrm{i}}(z,t),$$

$(k=\mathrm{s}, p_1, p_2, p_3)$, (1)

where $A_{k,\mathrm{i}}$ represents the slowly varying envelope of the optical field inside subsection of the SOA, k represents the input signal light and lasing light, $|A_{k,\mathrm{i}}|^2$ represents the optical power, $\alpha_{k,\mathrm{i}}$ is the chirp parameter which accounts for carrier-induced index changes, Γ is the mode confinement factor, α_{int} is the internal loss coefficient in SOA, $g_{k,\mathrm{i}}$ is the material gain of the SOA, P_{i} is the total optical power of inside subsection, and P_{sat} is the saturation power of the SOA. The amplified spontaneous emission (ASE) noise is depicted by two statistically independent Gaussian distributed random processes for $\mu_{k,\mathrm{i}}(z,t)$ which satisfies the following correlation[20]

$$\left\langle \mu_{k,\mathrm{i}}(z,t)\mu_{k,\mathrm{i}}^{*}(z',t')\right\rangle=\beta\Gamma R_{\mathrm{sp}}\delta(t-t')(v_{\mathrm{g}}E_{k}A_{\mathrm{cross}}),$$

$(k=\mathrm{s}, p_1, p_2, p_3)$, (2)

where β is the spontaneous coupling factor, R_{sp} is the spontaneous emission rate, v_{g} is the group velocity, E_k is the photo energy, and A_{cross} is the cross-sectional area of the active layer. The carrier density at each section obeys the following equation.

$$\frac{\mathrm{d}N_{\mathrm{i}}}{\mathrm{d}t}=\frac{I}{ewdL}-(c_1N_{\mathrm{i}}+c_2N_{\mathrm{i}}^2+c_3N_{\mathrm{i}}^3)-$$

$$g_{k,\mathrm{i}}\frac{G_{k,\mathrm{i}}-1}{\ln G_{k,\mathrm{i}}}\frac{|A_{k,\mathrm{i}}|^2\lambda_k}{hcwd},$$

$(k=\mathrm{s}, p_1, p_2, p_3)$, (3)

where I is the bias current of the SOA, c_1, c_2 and c_3 are recombination constants, w, d and L are width, depth and length of active region in SOA respectively, and $G_{k,\mathrm{i}}$ is the gain in each section.

$$\overline{g}_{k,\mathrm{i}}=\Gamma(g_{k,\mathrm{i}}-\alpha_{\mathrm{a}})-(1-\Gamma)\alpha_{\mathrm{c}}-\alpha_{\mathrm{scat}}, \quad (4)$$

$$G_{k,\mathrm{i}}=\exp(\overline{g_{k,\mathrm{i}}}l), \quad (5)$$

where l is the length of subsection. Due to the unidirectional transmission function of the optical isolator, the boundary condition of SFRL can be expressed as

$$A(0)=A(L)\varepsilon_1k_1k_2, \quad (6)$$

where ε_1 represents the loss of SFRL, excepting the loss of coupler1 and coupler2, while k_1 and k_2 indicate the proportion of coupler1 and coupler2 coupling into SFRL respectively. The evolution of phase Φ inside the SOA can be expressed as

$$\frac{\partial \Phi_i}{\partial z}=\frac{1}{2}\Gamma \alpha g_i. \tag{7}$$

The total change of the phase Φ_t can be calculated through by Eq.(7). The chirp of the lasing light is the first order derivative of the phase, which can be expressed as

$$\Delta f=-\frac{1}{2\pi}\frac{\mathrm{d}\Phi_t}{\mathrm{d}t}. \tag{8}$$

The transfer function of the Gaussian OBF is expressed as

$$H(\lambda)=T_{\max}\exp\left[-4\ln(2)(\frac{\lambda-\lambda_f}{B_{3dB}})^2\right], \tag{9}$$

where $T_{\max}$ is the maximum transmittance of filter, B_{3dB} represents the 3 dB bandwidth of filter, and λ_f represents the central wavelength of OBF.

Using the previously comprehensive broad-band dynamic model, we simulate all-optical broadcast UWB monocycle pulses based on XPM in SFRL. The parameters of the SOA are summarized in Tab.1 of Ref.[18]. The input signal is 10G Baud return-to-zero Gaussian pulse with full width at half-maximum (*FWHM*) of 48 ps. The signal symbol sequence is “1000000000” (the repetition rate of the symbol “1” is 1 GHz). The bias current of the SOA is 300 mA. The wavelengths of three lasing light are set to 1 544 nm, 1 546 nm and 1 548 nm, respectively. The wavelength of the signal light λ_s is set to 1 550 nm, and power of signal light is set to 6 dBm. k_1 and k_2 are set to 0.5 and 0.1. $T_{\max}$ and B_{3dB} are set to 0.95 and 0.32 nm.

We set the central wavelengths of OBF1, OBF2 and OBF3 to 1 544.22 nm, 1 546.22 nm and 1 548.22 nm, locating the wavelengths of the three lasing light in the positive slope region of OBF transfer function. Three UWB positive monocycle pulses can be produced at the output of the optical filters. The waveforms and corresponding radio frequency (RF) spectra are shown in Fig.2. It can be seen from Fig.2(a) that the shapes of three UWB positive monocycle pulses are similar and asymmetric. The widths of the positive pulses are 48 ps, while the widths of the negative pulses are 105 ps. Meanwhile, the amplitudes of the positive pulses are larger than those of the negative pulses. This is because that the carrier consumption in the SOA is faster than the recovery when the Gaussian pulse propagates in the SOA.

From Fig.2(b)—(d), we can see that the RF central frequencies of three UWB positive monocycle pulses are 4.95 GHz, 5 GHz and 4.95 GHz, with corresponding 10 dB bandwidths of 8.1 GHz, 8.2 GHz and 8.1 GHz. Thus the fractional bandwidths of three UWB positive monocycle pulses are 163.64%, 164% and 163.64%, respectively. In addition, the *PSDs* of three UWB positive monocycle pulses are in line with the FCC indoor spectrum mask. Therefore, the 10 dB bandwidths, fractional bandwidths and the *PSDs* of three UWB positive monocycle pulses all satisfy the FCC definition.

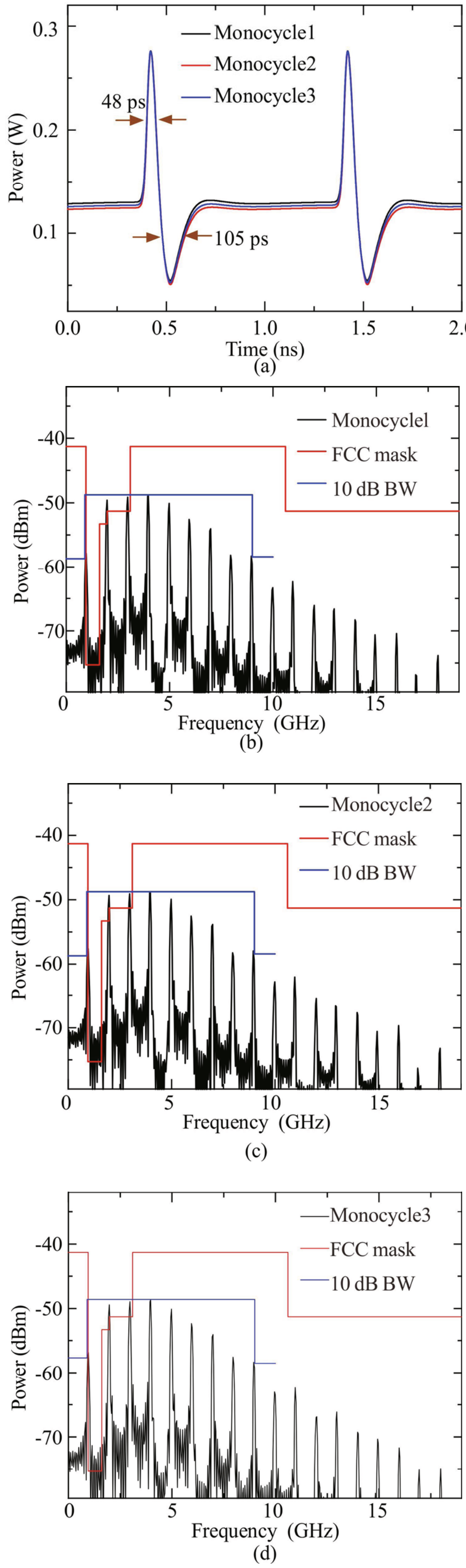

Fig.2 (a) Waveforms of three UWB positive monocycle pulses; Corresponding spectra of (b) monocycle1, (c) monocycle2, and (d) monocycle3

We set the central wavelengths of OBF1, OBF2 and OBF3 to 1 543.78 nm, 1 545.78 nm and 1 547.78 nm, locating the wavelengths of the three lasing light in the negative slope region of OBF transfer function while keeping the other parameters unchanged. Fig.3 shows the waveforms and spectra of three UWB negative monocycle pulses. Fig.3(a) shows that the shapes of three UWB negative monocycle pulses are also similar and asymmetric. The positive pulses of three UWB negative monocycle pulses are wider than those of the negative pulses (as shown in Fig.3(a), the widths of the positive pulses are 113 ps, while the widths of the negative pulses are 78 ps). This is also due to the faster carrier consumption in the SOA than the recovery when the Gaussian pulse propagates in the SOA. By comparing Fig.2 and Fig.3, it can be observed that the positive and negative monocycle pulses almost have the same average power (≈128 mW), and the shapes of three UWB negative monocycle pulses are the opposite of three UWB positive monocycle pulses. This is because that blue shift and red shift have the same offset ($\Delta\lambda$=0.22 nm), and the transfer function of the OBF is symmetric about its central wavelength.

Fig.3(b)—(d) show that the RF central frequencies of three UWB negative monocycle pulses are 3.25 GHz, 3.3 GHz and 3.3 GHz and corresponding 10 dB bandwidths are 5.1 GHz, 5.2 GHz and 5.4 GHz, indicating that the fractional bandwidths of three UWB negative monocycle pulses are 156.92%, 157.58% and 163.64%, respectively. The *PSDs* of all three UWB negative monocycle pulses also comply with the FCC indoor spectrum mask. Thus, the 10 dB bandwidths, the fractional bandwidths and the *PSDs* of all three UWB negative monocycle pulses also match the FCC definition. In addition, the UWB positive and negative monocycle pulses have similar spectrum envelope while the positive monocycle pulses have a higher *PSD*. Taking into account the FCC restrictions on the *PSD* of the UWB and the symmetry of the OBF transfer function, we only study the impact of system parameters on three UWB positive monocycle pulses.

The performance of three UWB positive monocycle pulses is investigated with different injection currents of the SOA. Fig.4(a)—(c) show the waveforms of three UWB positive monocycle pulses when the injection current of the SOA is set to 250 mA, 300 mA and 350 mA, respectively. We can see that the positive pulse amplitudes and average powers of three UWB positive monocycle pulses increase with the injection current of the SOA. It is because that the gain of the SOA increases as its injection current increases. In addition, the negative pulse amplitudes of three UWB monocycle pulses keep unchanged as the injection current of the SOA increases due to the carrier recovery characteristics of the SOA.

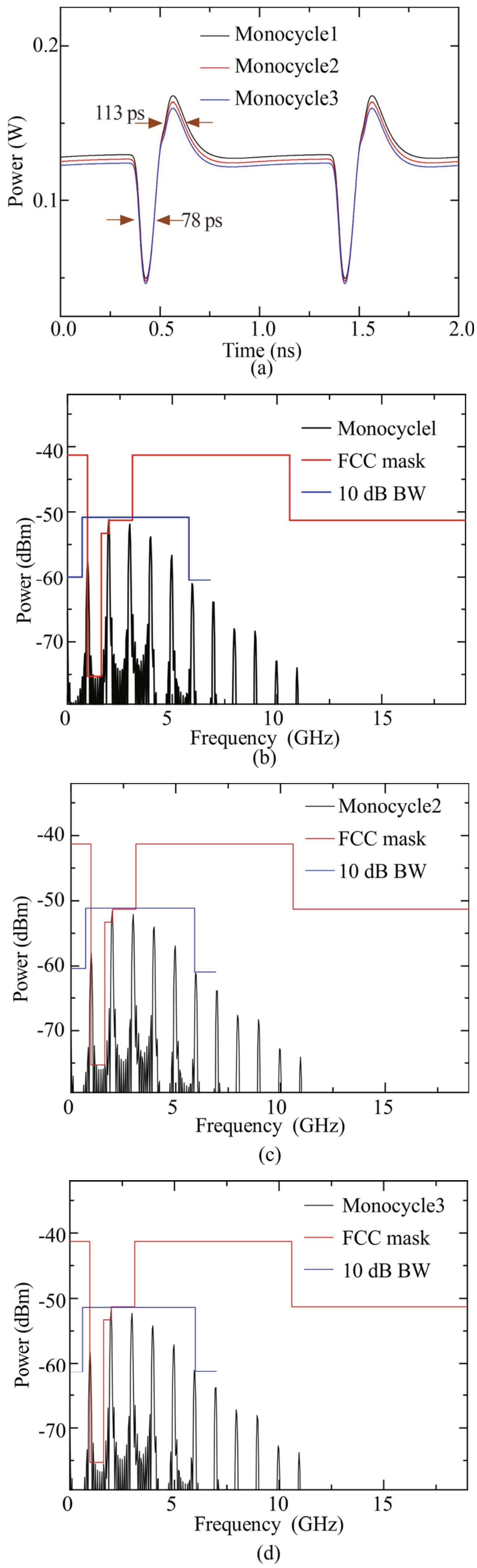

Fig.3 (a) Waveforms of three UWB negative monocycle pulses; Corresponding spectra of (b) monocycle1, (c) monocycle2, and (d) monocycle3

Fig.5(a) shows the RF central frequencies and 10 dB bandwidths of three UWB positive monocycle pulses in the case of different injection current of the SOA. The

RF central frequencies and the 10 dB bandwidths fluctuate slightly around 4.85 GHz and 8.2 GHz, indicating that the fractional bandwidths of three UWB positive monocycle pulses fluctuate slightly around 169.07%. Fig.5(b) shows that the *PSDs* of three UWB monocycle pulses increase slightly as the injection current of the SOA increases. The results show that when the injection current of the SOA varies from 250 mA to 350 mA, the *PSDs* of three UWB monocycle pulses all match the FCC regulation. Therefore, three UWB positive monocycle pulses generated by proposed scheme have a good tolerance to the injection current of the SOA.

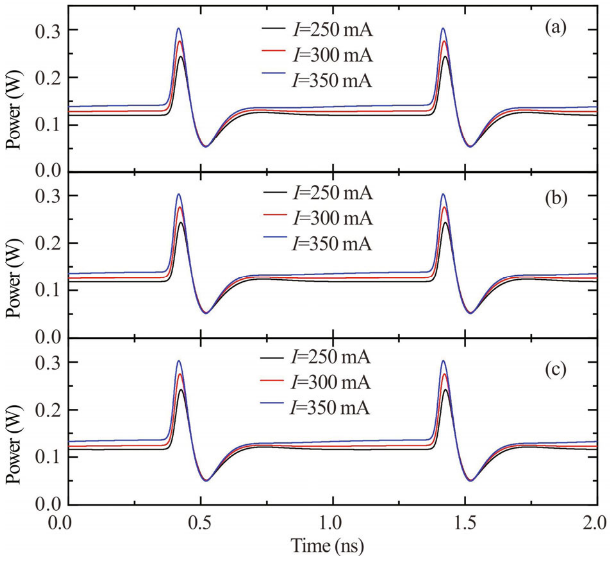

Fig.4 Waveforms of three UWB positive monocycle pulses in the case of different injection currents of the SOA: (a) Monocycle1; (b) Monocycle2; (c) Monocycle3

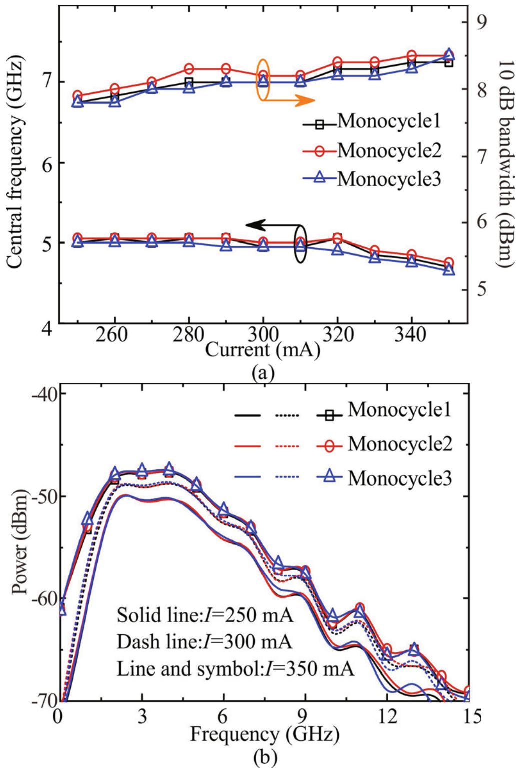

Fig.5 (a) RF central frequencies and 10 dB bandwidths and (b) RF spectrum envelopes of three UWB positive monocycle pulses in the case of different injection currents of the SOA

The waveforms of three UWB positive monocycle pulses are shown in Fig.6(a)—(c), with the power of signal light set to 2 dBm, 6 dBm and 10 dBm, respectively. It can be seen from Fig.6(a)—(c) that when the power of signal light is at a low level, the positive pulse amplitudes of three UWB monocycle pulses are very small, and the positive pulse amplitudes are smaller than the negative pulse amplitudes. This is because that the modulation strength of SOA is small when the power of signal light is weak, meaning that the carriers can be recovered quickly. More carriers will be consumed when the power of signal light increases gradually, indicating that the carrier consumption of the SOA is faster and the recovery is slower. Hence, the positive pulse amplitudes of three UWB monocycle pulses increase while the negative amplitudes pulse decrease, resulting that the positive pulse amplitudes of three UWB monocycle pulses become larger than the negative pulse amplitudes. Meanwhile, the average powers of three UWB monocycle pulses will decrease when the power of signal light increases, and the decrement becomes smaller as the power of signal light increases. This is because that the signal light will consume more carriers in the SOA as the power of signal light increases, indicating that the amplification of the SOA on the lasing light is reduced, and the effect of the power of signal light on the SOA gain will no longer be significant when the SOA gain is close to saturation.

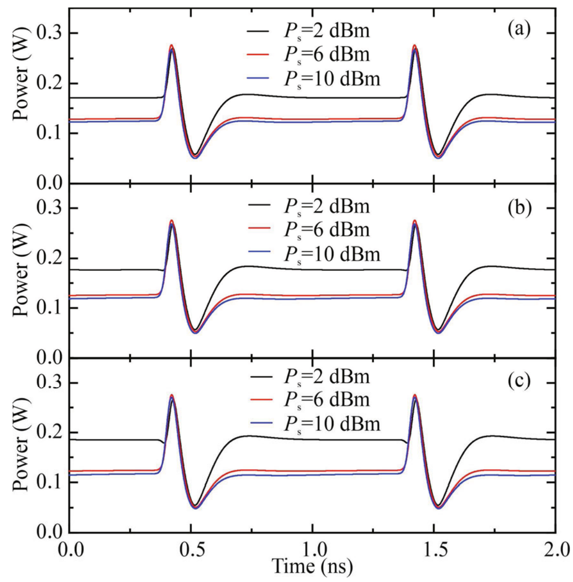

Fig.6 Waveforms of three UWB positive monocycle pulses in the case of different signal light powers: (a) Monocycle1; (b) Monocycle2; (c) Monocycle3

Fig.7(a) illustrates the RF central frequencies and

10 dB bandwidths of three UWB positive monocycle pulses in the case of different signal light powers. When the power of signal light varies from 2 dBm to 10 dBm, the central frequencies and 10 dB bandwidths have the same trend of change. Both the RF central frequencies and 10 dB bandwidths increase first, and then remain unchanged. This is because that when the power of signal light reaches a certain value that makes the SOA gain saturation, then the modulation depth of SOA will no change significant. Fig.7(b) shows the RF spectrum envelope when the power of signal light is set to 2 dBm, 6 dBm and 10 dBm, respectively. The low frequency component of the spectrum is lower when the input signal power is at a high level, which matches the FCC mask better. Therefore, three UWB positive monocycle pulses with better performance can be obtained when the power of signal light is not less than 4 dBm.

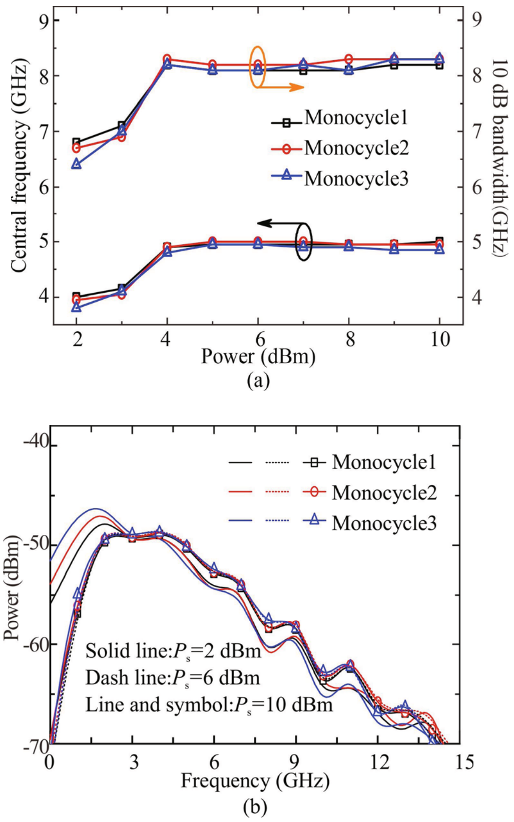

Fig.7 (a) RF central frequencies and 10 dB bandwidths and (b) RF spectrum envelopes of three UWB positive monocycle pulses in the case of different signal light powers

Fig.8 depicts the RF central frequencies and 10 dB bandwidths of three UWB positive monocycle pulses as a function of the wavelength of signal light. From Fig.8, we can observe that the RF central frequencies and 10 dB bandwidths change slightly as the wavelength of signal light varies from 1 540 nm to 1 560 nm excluding the wavelengths of lasing light. The central frequencies and the 10 dB bandwidths of three UWB positive monocycle pulses fluctuate slightly around 4.75 GHz and 8.25 GHz, indicating that the fractional bandwidths of three UWB monocycle pulses fluctuate slightly around 173.68%. Hence, three UWB positive monocycle pulses also have a good tolerance to the wavelength of signal light.

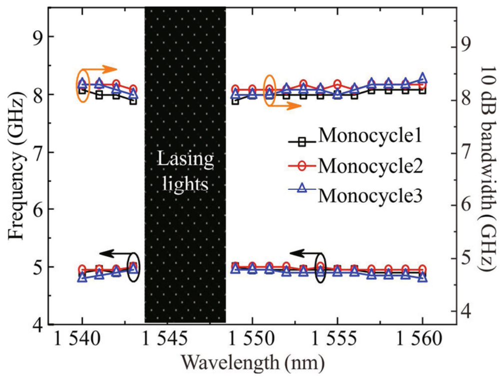

Fig.8 RF central frequencies and 10 dB bandwidths of three UWB positive monocycle pulses as a function of the wavelength of signal light

Fig.9 shows the waveforms and corresponding RF spectrum envelopes of three UWB positive monocycle pulses when k_2 is set to 0.1, 0.2 and 0.4, respectively. Form Fig.9(a), it can be observed that three UWB positive monocycle pulses almost have the same average power and shape when k_2 is set to 0.1 and 0.2. It is because that the power of lasing light coupled into SFRL is weak when k_2 is set to a small scale, the carriers in SOA are mainly consumed by the signal light resulting that the gains of three UWB positive monocycle pulses are suppressed. The interaction between signal light and three lasing light in the SOA is mainly XPM, the phase change of three lasing light all determined by the shape of the signal light resulting three UWB positive monocycle pulses with similar intensity shape after conversion. It also can be seen form Fig.9(a) that the average power of three UWB positive monocycle pulses with k_2 set to 0.2 is lower than 0.1. It is because that the proportion of three UWB positive monocycle pulses power to the input power of coupler2 has dropped (from 0.9 to 0.8). The average powers of three UWB positive monocycle pulses are significantly different when k_2 is set to 0.4. This is because that the power of the lasing light coupled into the SOA increases resulting that the lasing light starts to consume carriers in the SOA and is amplified, but the gains of the SOA for different wavelengths are different. In addition, a positive Gaussian pulse generated on the right side of positive monocycle pulse. This is because the phases of a lasing light are also modulated by other lasing light and itself when the powers of lasing light coupled into the SOA are strong. From Fig.9(b), it can be seen that the *PSDs* of all three UWB negative monocycle pulses no longer comply with the FCC indoor spectrum mask when k_2 is set to 0.4. Hence, in order to obtain three

UWB positive monocycle pulses with better performance, the powers of the lasing light coupled to the SFRL should not be strong, which can be achieved by adjusting the ratio of k_1 or k_2. Reducing k_2 not only decrease the powers of the lasing light coupled to the SFRL but also increase the output power of three UWB monocycle pulses improving the power conversion efficiency.

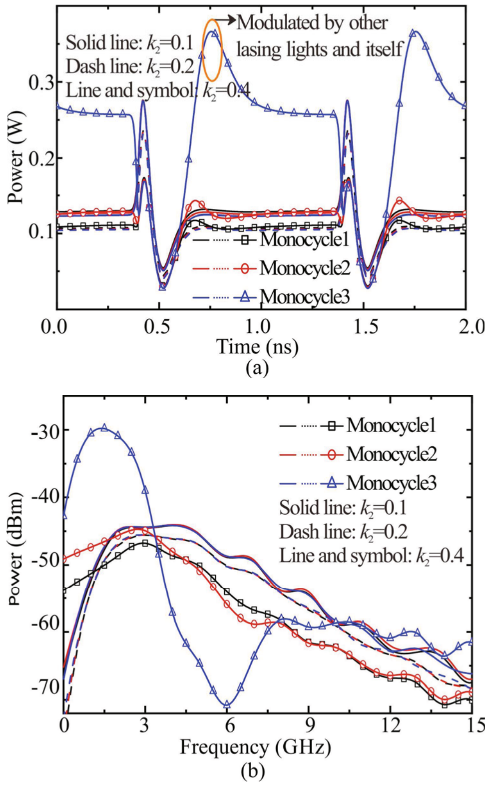

Fig.9 (a) Waveforms and (b) corresponding RF spectrum envelopes of three UWB positive monocycle pulses in the case of different k_2

A novel approach to all-optical generate broadcast UWB monocycle pulses based on XPM in the SFRL is proposed and a comprehensive broad-band dynamic model of this kind of all-optical broadcast UWB monocycle sources is established. Three UWB positive and negative monocycle pulses which match the FCC definition can be obtained by setting the central frequencies of OBFs. The impacts of injection current of SOA in the SFRL, the power and wavelength of signal light, the powers of lasing light coupled into SFRL on the performance of the UWB positive monocycle pulses with *PSD* are analyzed. The results show that three UWB positive monocycle pulses with better performance can be obtained when the power of signal light is larger than 4 dBm, and three UWB positive monocycle pulses have a good tolerance to both the injection current of the SOA and the wavelength of the signal light. The powers of lasing light coupled into SFRL have a significant impact on the output three UWB positive monocycle pulses, and they should not be strong.

Statements and Declarations

The authors declare that there are no conflicts of interest related to this article.

References

[1] WIN M Z, SCHOLTZ R A. Ultra-wide bandwidth time-hopping spread-spectrum impulse radio for wireless multiple-access communications[J]. Transactions on communications, 2000, 48(4): 679-691.

[2] PORCINO D, HIRT W. Ultra-wideband radio technology: potential and challenges ahead[J]. Communications magazine, 2003, 41(7): 66-74.

[3] GUENNEC Y L, GARY R. Optical frequency conversion for millimeter-wave ultra-wideband-over-fiber systems[J]. Photonics technology letters, 2007, 19(13): 996-998.

[4] SHEHATA M, MOSTAFA H, ISMAIL Y. On the theoretical limits of the power efficiency of photonically generated IR-UWB waveforms[J]. Journal of lightwave technology, 2018, 36(10): 2017-2023.

[5] MU H Q, WANG M G, LI M. Power-efficient FCC-compliant UWB generator using polarization maintaining FBG-based spectral shaper and incoherent wavelength-to-time mapping[J]. Optical fiber technology, 2019, 50(1): 271-276.

[6] MORENO V, RIUS M, MORA J, et al. Scalable UWB photonic generator based on the combination of doublet pulses[J]. Optics express, 2014, 22(13): 15346-15351.

[7] YANG C L, LI X, FU S N, et al. A UWB pulse generation based on a phase modulator and programmable filter[J]. Optics communications, 2014, 318(1): 166-170.

[8] MALEKIZANDI M, LE Q T, EMSIA A, et al. Generation of UWB doublet pulse based on directly modulated laser and chromatic dispersion[J]. Photonics technology letters, 2016, 28(3): 343-346.

[9] SHAO J, LIU S H. Photonic generation of filter-free ultrawideband monocycle and doublet signal using single semiconductor optical amplifier in counter-propagation scheme[J]. Optical engineering, 2016, 55(2): 026117.

[10] TAKI H, AZOU S, HAMIE A, et al. On phaser-based processing of impulse radio UWB over fiber systems employing SOA[J]. Optical fiber technology, 2017, 36(1): 33-40.

[11] HU Z F, XU J H, HOU M. Theoretical demonstration of all-optical switchable and tunable UWB doublet pulse train generator utilizing SOA wavelength conversion and tunable time delay[J]. Frontiers of optoelectronics, 2017, 10(2): 180-188.

[12] GHAFOOR S. Polarization multiplexing-based ultrawideband over fiber communication employing direct modulation and carrier re-use[J]. Communications letters, 2019, 23(6): 1008-1011.

[13] DU C, LIU F M, LI X, et al. UWB quadruplet signal

generation based on a DP-QPSK modulator and a delay-line filter[J]. Applied optics, 2020, 59(14)：4404-4409.

[14] HUANG K, ZHANG S G, MA X R, et al. Monocycle and doublet pulses generation via photon echo in rare earth-doped optical crystal[J]. Optical engineering, 2016, 55(12)：126109.

[15] DU C, WANG Y, WANG D, et al. Photonic generation of millimeter-wave ultra-wideband monocycle signal using up-conversion based on stimulated Brillouin scattering effect[J]. Optical and quantum electronics, 2019, 51(1)：25.

[16] ZHANG F Z, WU J, FU S N, et al. Simultaneous multi-channel CMW-band and MMW-band UWB monocycle pulse generation using FWM effect in a highly nonlinear photonic crystal fiber[J]. Optics express, 2010, 18(15)：15870-15875.

[17] ZHAO Z S, LI P L. Research of all-optical broadcast UWB signal source based on semiconductor fiber ring laser[J]. Acta physica sinica, 2019, 68(14)：140401. (in Chinese)

[18] ZHAO Z S. Research of all-optical broadcast doublet signals based on semiconductor fiber ring laser[C]//2019 IEEE 11th International Conference on Communication Software and Networks, June 12-19, 2019, Chongqing, China. New York：IEEE, 2019.

[19] DONG H, ZHU G, WANG Q, et al. Multi-wavelength fiber ring laser source based on a delayed interferometer[J]. Photonics technology letters, 2005, 17(2)：303-305.

[20] REALE A, CARLO A D, LUGLI P. Gain dynamics in traveling-wave semiconductor optical amplifiers[J]. Journal on selected topics in quantum electronics, 2001, 7(2)：293-299.